MICHIGAN STATE
U N I V E R S I T Y

National Superconducting Cyclotron Laboratory

DISSOCIATION OF ^{6}He
Submitted to Phys. Rev. C

**J. WANG, A. GALONSKY, J.J. KRUSE, E. TRYGGESTAD,
R.H. WHITE-STEVENS, P.D. ZECHER, Y. IWATA, K. IEKI,
Á. HORVÁTH, F. DEÁK, Á. KISS, Z. SERES, J.J. KOLATA,
J. von SCHWARZENBERG, R.E. WARNER, H. SCHELIN**

NSCL

DISSOCIATION OF ^{6}He
Submitted to Phys. Rev. C

J. Wang[*], A. Galonsky, J.J. Kruse[†], E. Tryggestad, R.H. White-Stevens[‡], and P.D. Zecher[§]

National Superconducting Cyclotron Laboratory and Department of Physics and Astronomy,

Michigan State University, East Lansing, Michigan 48824-1321

Y. Iwata[**] and K. Ieki

Department of Physics, Rikkyo University, 3 Nishi-Ikebukuro,

Toshima, Tokyo 171-8501, Japan

Á. Horváth , F. Deák, and Á. Kiss

Department of Atomic Physics, Eötvös Loránd University, Pázmány P. sétány 1/A, H-1117

Budapest, Hungary

Z. Seres

KFKI Research Inst. for Particle and Nuclear Physics, Konkoly-Thege út 29-33, P.O. Box 49,

H-1525 Budapest 114, Hungary

J.J. Kolata and J. von Schwarzenberg[∞]

Department of Physics, University of Notre Dame, Notre Dame, Indiana 46556-5670

R.E. Warner

Department of Physics, Oberlin College, Oberlin, Ohio 44074

H. Schelin

CEFET, Av. Sete de Setembro 3165 80230-901, Curitiba, Pr, Brazil

[*] Present address: American Express Co., 3WFC, 4502, 200 Vesey Street, New York, NY 10285.

[†] Present address: Radiation Oncology, Mayo Clinic, 200 First St. SW, Rochester, MN 55905.

[‡] Summer REU student.

[§] Present address: Investor Analytics LLC, 630 Fifth Avenue Suite 1919, New York, NY 10111.

[**] Present address: National Inst. of Radiological Sciences, 4-9-1 Anagawa, Inage, Chiba 263-8555, Japan.

[∞] Present address: University of Vienna, Waehringer Strasse 17, A-1090 Vienna, Austria

Abstract

The dissociation reaction ^{6}He $\rightarrow$ α + 2n was studied with ^{6}He projectiles at 23.9 MeV/u in targets of C, Al, Cu, Sn, Pb and U. Relative to Al, the 2n removal cross section σ_{-2n} with each of the other targets was determined. With U, the Coulomb part accounts for 2/3 of σ_{-2n}. The widths of the α-particle and neutron parallel momentum distributions increase with target Z. For the α-particle, ^{6}He dissociation on C gave width σ = (40.2 $\pm$ 2.3) MeV/c, corresponding to an rms radius of the halo neutrons of (2.95 $\pm$ 0.17) fm — (0.35$\pm$ 0.17) fm larger than the rms radius of all four neutrons. The relation between the widths of the α-particle and neutron distributions indicates only a small correlation between the two neutrons. This conclusion is supported by the distribution function for the angle between the two neutrons, which was obtained in kinematically complete measurements. The latter measurements with the U target also yielded an E1 strength function, and it agreed with one determined in an experiment at ten times our beam energy.

I. INTRODUCTION

A neutron halo nucleus has one or more neutrons that are so lightly bound that their wave function extends well beyond the rest of the nucleus. Such nuclei are found near the neutron dripline. Examples are ^{11}Be, with a one-neutron halo, and ^{6}He and ^{11}Li, with two-neutron halos. When a halo nucleus is used as a projectile, the halo manifests itself by producing a larger reaction cross section than do neighboring nuclei [1], with the obvious interpretation that the radius of a halo nucleus is enhanced. A dominant channel in the reaction of a halo nucleus is the separation of the halo neutron(s) from the remainder of the nucleus. The momentum distribution of either the remainder or of the neutron has been found to be narrower than those of normal nuclei, suggesting again a large spatial distribution of the nuclear matter [2].

These observations led to the picture of a halo nucleus as a lightly-bound structure consisting of two parts—a core and a neutron (or neutron pair) [3,4]. A consequence of this binary structure is the possibility of Coulomb exciting the structure into an oscillation of the core against the halo neutron(s) [4]. In comparison to the giant dipole resonance, the excitation energy of this resonant mode would be rather low because the restoring force on the core would be supplied by only the one or two halo neutrons rather than by all the neutrons in the nucleus. Hence, the word *soft* precedes *dipole resonance* in the name of this mode. What has been observed, whenever looked for, is a peak in the electric dipole strength function at an energy less

than a few MeV above the dissociation threshold [5,6,7].

One may expect similar structure and properties for all nuclei near the neutron dripline. Apart from the deuteron, the ^{6}He nucleus is the lightest of the halo nuclei, and with an α-particle for its core, it should also be the simplest; its study may contribute to the understanding of the properties of other dripline nuclei as well as of itself. When ^{6}He is excited to an energy above the 2-n separation energy of 0.975 MeV, the three-body decay ^{6}He $\rightarrow$ α + n + n may occur. A brief review of the medium- and high-energy literature on ^{6}He begins with Tanihata et al. [1] who measured the interaction cross sections of ^{6}He at 0.79 GeV/u on Be, C and Al targets, from which the nuclear interaction radius was deduced. Then, Kobayashi et al. [8,9] measured the interaction cross sections of ^{6}He around 1 GeV/u and the transverse momentum distribution of the α-particle from the fragmentation of ^{6}He. Later, the transverse momentum distributions of neutrons from ^{6}He at 0.8 GeV/u on Pb and C targets were measured by the same group [10]. The momentum distribution of the α-particle from ^{6}He fragmentation, detected at 5° for beam energies near 65 MeV/u, was measured [11]. The early studies of neutron halo nuclei have been reviewed [12, 13]. In 1996 total reaction cross sections of ^{6}He at intermediate energies (20-40 MeV/u) were reported [14]. An experiment was performed recently to study the one-neutron stripping mechanism of ^{6}He at 240 MeV/u [15], and a similar group reported on inelastic excitations of ^{6}He [16]. Last year the soft dipole resonance was observed in the ^{6}Li(^{7}Li,^{7}Be)^{6}He reaction at 65 MeV/u [17].

The experiment reported here is on dissociation of ^{6}He. The data deal with four aspects of the structure of ^{6}He: (1) The cross section for the dissociation σ_{-2n}, in combination with previously-measured [18] reaction cross sections for ^{6}He and the α-particle, provide a test of the core-2n model of ^{6}He. Also, by using both low-Z and high-Z targets, we were able to separate the Coulomb and nuclear contributions to the dissociation. (2) Measurements of the parallel momentum distributions of the α-particle gave a value for the rms radius of the halo neutrons. (3) A measure of the correlation between the two halo neutrons was obtained from two kinds of data—the momentum distribution of the α-particle in comparison with the momentum distribution of the neutrons, and the distribution of the angle between the neutrons. (4) From kinematically complete data and the Coulomb fraction determined in (1) above, we were able to measure the first few MeV of the E1 strength function. After a description of the experimental setup, each of these four aspects is presented in order.

II. EXPERIMENTAL SETUP

A ^{6}He beam of 25.2 MeV/u was produced with the K1200 cyclotron and A1200 fragment separator [19] at the National Superconducting Cyclotron Laboratory at Michigan State University. The beam delivered to the targets consisted of 81% ^{6}He and 19% ^{9}Be, and the intensity was about 10^4/s. The ^{9}Be particles were distinguished from ^{6}He particles by their time of flight over a path of 41.5 m between a thin plastic scintillator placed just after the A1200 separator and one of 16 plastic scintillator bars which constitute the E detectors of Fig. 1.

That figure shows the remainder of the experimental setup. The direction of each ^{6}He incident on the target was determined to ~ 0.2° FWHM by two position-sensitive parallel-plate
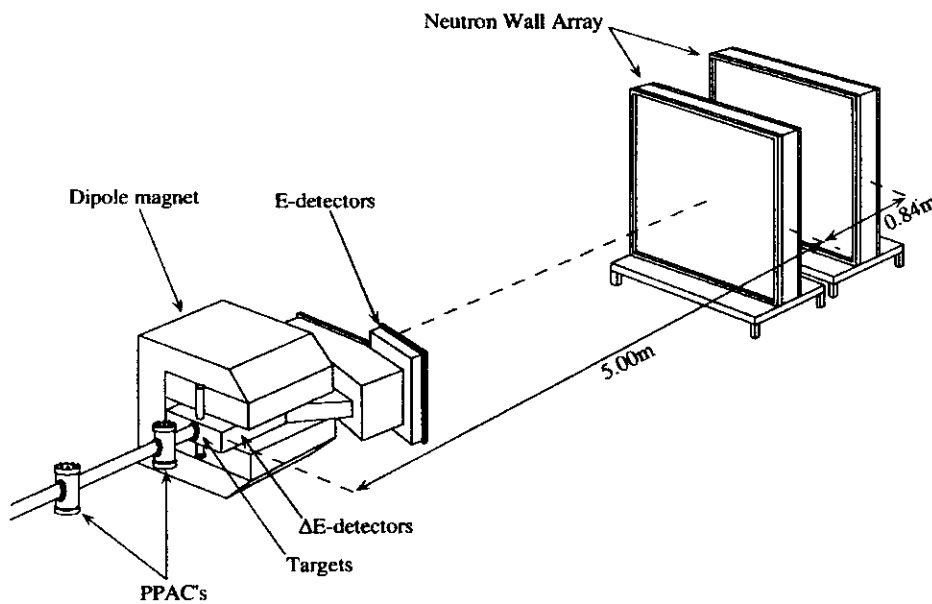

Fig. 1 Schematics of the experimental setup. The neutron walls, one behind the other, were placed 5.00 and 5.84 meters from the target. A plastic scintillator array (E detectors) was mounted inside the vacuum chamber about 1.8 meters from the target. Silicon strip detectors (ΔE detectors) were located at the entrance of the magnet, 15.2 cm from the target. PPACs were mounted 39 and 130 cm upstream from the target.

avalanche counters (PPAC's) [20] positioned 39 cm and 130 cm upstream from the targets. The experiment was performed with six targets—C, Al, Cu, Sn, Pb and U— whose thicknesses were 94, 237, 274, 373, 384 and 344mg/cm^2, respectively. We also took a run with a blank target in order to see events from anything other than the targets. For this run the beam energy was reduced by 2.6 MeV/u, the typical energy loss in the targets.

Neutrons in the experiment were detected by a pair of neutron walls [21] with active area 2m × 2m. Each wall consisted of 25 horizontally stacked, rectangular Pyrex cells filled with NE-

213 liquid scintillator and with photomultiplier tubes (PMT) attached to their ends. Neutron time-of-flight was obtained from the time signal of the coincident α-particle in the E detector and the mean time of the two PMT signals. Horizontal position of the neutron was determined from the time difference between the two PMT signals. For a 25-MeV neutron the energy resolution is ~ 4% FWHM, and one wall has an efficiency of ~ 11% if a threshold of 1 MeV electron equivalent energy is set for the two phototubes at the ends of a cell.

The fragment detection system [22] consists of two silicon ΔE detectors, a deflecting magnet and 16 scintillator bars (E detectors). The magnet reduces background by deflecting unreacted projectiles (^{6}He in this experiment) away from the beamline into a scintillator bar so that most neutrons produced by the stopping ^{6}He are directed away from the neutron walls. A neutron shield, not shown in Fig. 1, was interposed between the bars and the walls. By varying the magnetic field we deflected an α-particle beam into each scintillator bar for energy calibration purposes.

Each ΔE detector, 5cm x 5cm x 250μm, was a MICRON 16x16 double-sided silicon strip detector. The strip detectors were 15.2 cm from the target. The two Si detectors were placed side-by-side, giving horizontal and vertical acceptances of 36° and 19° for the pair.

III. 2N REMOVAL CROSS SECTION σ_{-2n}

A sample of the basic data is shown in Fig. 2, where we see pulse height spectra in 12 of the 16 scintillator bars in coincidence with a neutron; the target was U. The sharp peaks around channel 250 are from unreacted ^{6}He projectiles in accidental coincidence with neutrons. Most of these events are in Bars # 5 and 6. Coincidence with a neutron has reduced the number by almost a factor of 1,000. The bar number increases with magnet deflection angle, and starting with Bar #8 we see the lower-rigidity α-particles increase in intensity to a maximum in Bar # 11 and then fall off. Kinematic spread in ^{6}He breakup is the main cause of the width of the α-particle peaks. From these spectra it is easy to count the number of α- particles in spite of the fact that they are only ~ 10^{-4} of the particles entering the magnetic field from the target.

From the integrated α-particle counts in Bars 8-14 and ^{6}He counts in Bars 3-8 in Fig. 2 and in similar spectra for the other targets we determined the relative values of σ_{-2n}. To get absolute values we normalized the Al value to σ_{-2n} of ^{6}He on Si, measured by Warner et al. [14] to be
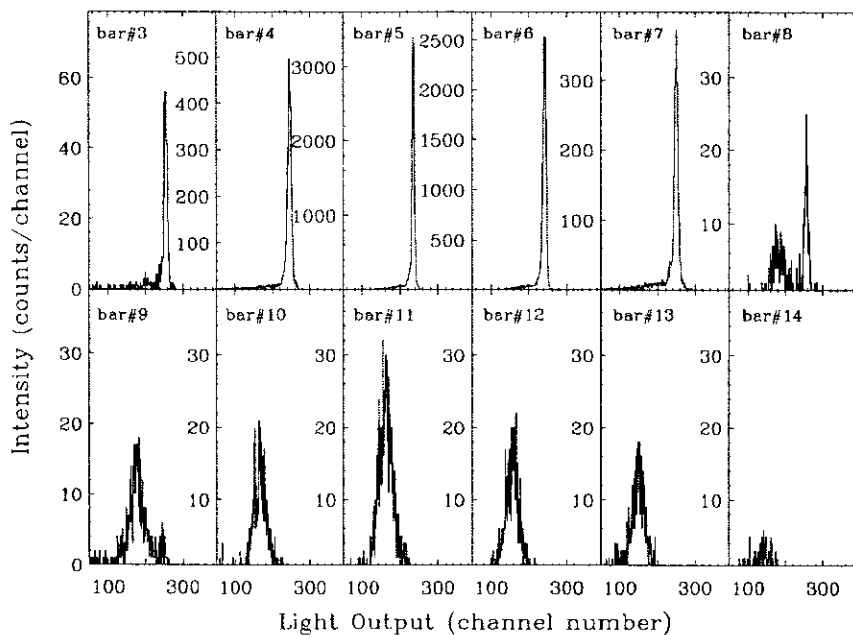
Fig. 2. Light output distributions in scintillator bars 3-14 for the U target. The sharp peak in Bars 3-8 are unreacted ^{6}He projectiles. The broad peak in Bars 8-14 are α-particles. Note the different intensity scales.

(0.47 ± 0.06) b. The σ_{-2n} values for all of the targets are listed in the second column of Table I, and two Glauber predictions are given in the third and fourth columns. Glauber calculations of reaction cross sections were first applied to data at bombarding energies near 1 GeV/nucleon [23], where they are most rigorously justified. However, they were also found to predict well the magnitude and energy dependences of σ_R and σ_{-2n} data at bombarding energies near 50

Table I. Values of σ-2n in barns. In addition to the given statistical errors on the measured values, there is a 13% systematic error since the cross sections for five of the targets were determined relative to 0.47 ± 0.06 for Si [14] and Al. The third, fourth and last columns give the results of model calculations; columns 2 and 5, present experiment.

Target	Measured Here	Warner [18]	Ferreira et al. [25]	Coulomb σ-2n	Warner [18]
U	1.87 ± 0.10	1.69		1.25± 0.17	1.10
Pb	1.70 ± 0.10	1.51	1.80	1.02± 0.14	0.92
Sn	1.22 ± 0.07	0.92		0.42± 0.06	0.39
Cu	0.82 ± 0.05	0.62	0.89	0.16± 0.02	0.15
Al	0.47	0.43		0.037± 0.005	0.04
C	0.36 ± 0.025	0.35	0.46	0.009± 0.001	0.01

MeV/nucleon [18]. The predictions in the third column of Table I were made following identically the method used in Ref. [18] with matter densities taken from [24]. The result given by Ferreira et al. [25] is somewhat different. Most of the difference is in the calculation of the nuclear cross section since both authors used the same model to obtain the Coulomb cross section. The ^{6}He projectile energy in Ferreira's calculations is 30 MeV/u, but we adapted Warner's code [18] to our energy of 23.9 MeV/u; it is probably the better one for comparison with our data. For all targets, Warner's predictions are below our measured values, and Ferreira's are above them.

A test of the core-2n model [26] applied to ^{6}He is to check whether

$$\sigma_R(^6He + T) = \sigma_R(\alpha + T) + \sigma_{-2n}(^6He + T).\qquad(1)$$

The simple additivity in Eq. 1 says that quantum mechanical interference is negligible for interactions of core+halo nuclei. There are two reaction (R) cross sections and one target (T), and, of course, the projectile velocity should be the same throughout. A test is available for the Pb target since σ_R has been determined [18] to be (4.51 ± 0.10) barns for ^{6}He and (2.69 ± 0.08) b for α. The difference, (1.82 ± 0.13) b, compares well with our measurement of (1.70 ± 0.10) b for $\sigma_{-2n}(^6He + Pb)$ in Table I. The three projectile velocities in Eq. 1 are not exactly the same in this test, but [18] shows only a small velocity dependence.

3.1   Coulomb contribution

The purpose of using both low-Z and high-Z targets in the experiment was to separate the Coulomb and nuclear contributions to σ_{-2n}. To perform this separation we used the expected nuclear and Coulomb dependencies on A and Z:

$$\sigma_{-2n} = \sigma_{nuclear} + \sigma_{coulomb} = a(1.2A^{1/3} + 2.6) + bZ^{1.8}\qquad(2)$$

The nuclear part is assumed to proceed *via* peripheral collisions, hence the proportionality to the sum of the target and ^{6}He radii [27, 28]. The Coulomb part depends on the intensity $n_{E1}(Z, E_\gamma)$ [29] of equivalent E1 photons surrounding the target nucleus. If one examines $n_{E1}(Z, E_\gamma)$ *vs.* Z,A for the six targets in the region covered by our experiment ($E_\gamma \sim$ 1-3 MeV), one finds to good approximation that $n_{E1}(Z, E_\gamma) \propto Z^{1.8}$. The increasing distance of closest approach with A (and Z) prevents the dependence from being Z^2. The σ_{-2n} data, and the best fit to them, are shown in Fig. 3 with $a = 0.0734 \pm 0.0065$ barns and $b = (3.66 \pm 0.50) \times 10^{-4}$ barns. Hence, the Coulomb cross sections, which are also listed in Table I and are the dot-dashed curve in Fig. 3, are given by:

$$\sigma_{Coulomb} = (3.66 \pm 0.50)10^{-4} Z^{1.8} \text{ barns.} \qquad (3)$$
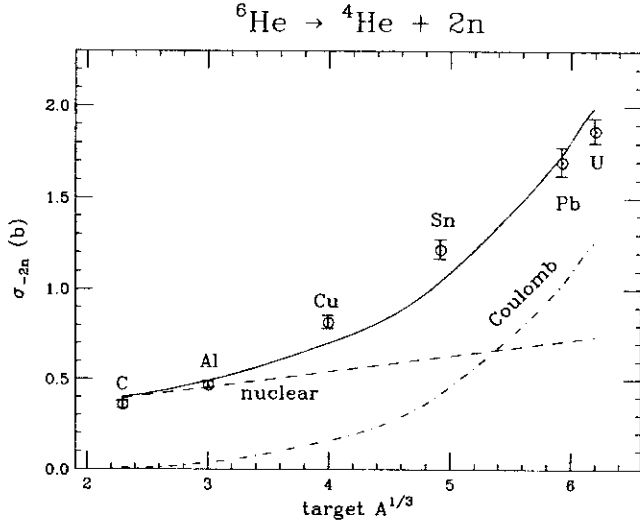

Fig. 3. Total 2n removal cross sections for the six targets. The points are the experimental data. The solid curve is a fitting model to extract the Coulomb part of the cross section (Eq. 3). The results are also listed in Table I.

It can be seen that for U and Pb the Coulomb effect accounts for more than half of the total 2-n removal cross section of ^{6}He. The essential agreement between our measurement and Warner's calculations [14, 18] may mean that his matter densities, nucleon-nucleon cross sections, and E1 strength functions are realistic.

IV. MOMENTUM DISTRIBUTIONS and HALO RADIUS

The Serber model [30] tells us that the measured momentum distribution of a fragment or neutron resulting from a "sudden" dissociation is the same as the momentum distribution of that component in the ^{6}He projectile. In our experiment the beam velocity is ~ c/4, and the interaction time with a nucleus in the C target ~ 50 fm/c, whereas a halo neutron orbit has a radius of ~ 3 fm (see below), a momentum of ~ 40 MeV/c (see Table II below) and, therefore, a period of ~ 400 fm/c. Hence, the interaction time is much less than the period of the motion, and the sudden approximation is valid. That validity means that a measurement of momentum distribution will, by means of a Fourier transform, give a spatial distribution. To study the 2n halo, we use the momentum distribution of the α-particle, which, by momentum conservation is the same as that of the two neutrons but does not require an n-n coincidence measurement. In fact, we used the distribution of only the parallel component of the α-particle momentum because Coulomb deflection of the incident ^{6}He and of the released α-particle increases the transverse momentum but has little effect on the parallel component for the small angles of this experiment.

Following Hansen and Jonson [4], we use the simple Yukawa-type wave function to obtain the asymptotic behavior of the wave function, where peripheral reactions are strong:

$$\psi(r) \propto \frac{1}{\sqrt{2\rho\pi}} \frac{e^{-r/\rho}}{r} \quad , \tag{4}$$

where ρ is a size parameter and r is the distance between the α-particle core and each halo neutron. After Fourier transforming $\psi(r)$ and integrating over the two transverse dimensions, the parallel momentum distribution has the form

$$\frac{dN}{dp} = \frac{\Gamma/2}{(p-p_0)^2 + (\Gamma/2)^2} \quad , \tag{5}$$

with maximum at p_0 and FWHM $= \Gamma = \dfrac{2\hbar}{\rho}$. This distribution and a Gaussian with the same

FWHM are almost identical in the central region, so the width σ of the equivalent Gaussian can be used to determine the rms halo radius:

$$\langle r^2 \rangle^{\frac{1}{2}} \approx \frac{\rho}{\sqrt{2}} = \frac{2\hbar}{2.354\sigma\sqrt{2}} \quad . \tag{6}$$

For all six targets the parallel momentum distribution of the α-particles is well fitted with a Gaussian. As a representative sample, we show the distribution and fit with the U target in Fig. 4.
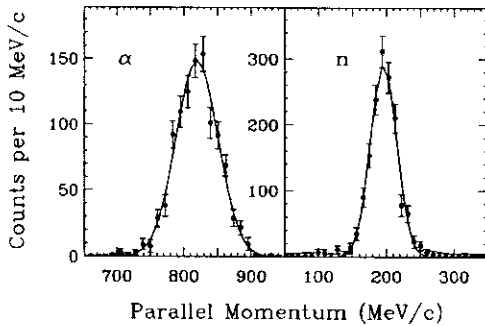

Fig. 4. Alpha particle and neutron parallel momentum distributions from ^{6}He breakup on U. The curves are Gaussians.

The width (σ values) for each target is listed in Table II and plotted against the Z of the target in

Table II. Widths, in MeV/c, of the parallel momentum distributions for the six targets.

	C	Al	Cu	Sn	Pb	U
$\sigma_{P//}(\alpha)$	40.2±2.3	44.6±2.2	33.1±1.6	33.0±1.3	32.4±1.4	31.2±0.9
$\sigma_{P//}(n)$	26.9±2.2	24.7±1.4	21.9±1.5	23.0±1.3	19.8±1.2	19.5±1.0

the top part of Fig. 5. (For use in the next section, Sec. V, the same information for neutrons is included in Figs. 4 and 5 and in Table II.) It can be seen that the widths of both the neutron and the α-particle distributions decrease with increasing target charge. Perhaps the decrease may be
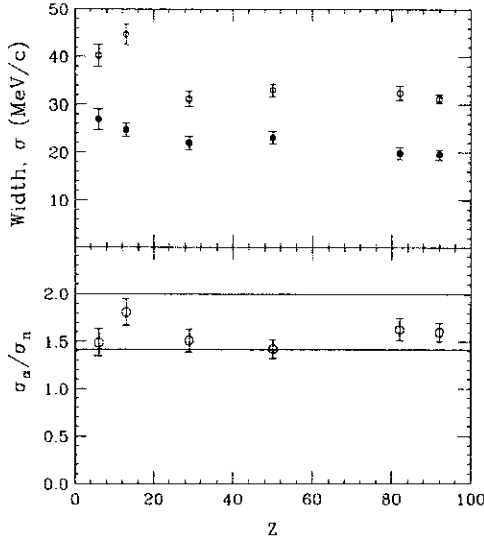

Fig. 5 (top) Widths of α-particle (open points) and neutron (filled points) parallel momentum distributions for the six targets. (bottom) Ratio of the above widths compared to $\sqrt{2}$ and 2.

attributed to a weakening of the validity of the sudden approximation when the long-range Coulomb interaction makes a significant contribution to the breakup, since long range implies long interaction time. Then the distributions with the C target should most reliably give the distributions within ^{6}He. Using $\sigma_\alpha = (40.2\pm2.3)$ MeV/c for the C target, Eq. 6 implies that

$$\left\langle r^2 \right\rangle^{\frac{1}{2}} \approx (2.95 \pm 0.17) fm.$$

The rms radius of all four neutrons in ^{6}He has been determined from ^{6}He interaction cross sections [1] to be (2.61 ± 0.03) fm [27] and (2.59 ± 0.04) fm [28]. The rms radius determined here from the α-particle parallel momentum distribution reflects only the two halo neutrons because the calculation is based upon an asymptotic wave function. Therefore, the rms radius determined here should be larger, and it is, by (0.35 ± 0.17) fm.

Many refinements have been made in computing the matter density of ^{6}He. Csótó [31] included a t + t configuration and found 2.65 fm for the neutron radius. Arai et al. [32] allowed the α-particle core to have a 3N + N cluster and for various models got neutron radii in the range 2.57-2.77 fm. Oganessian et al. [33] applied a three-body calculation using the method of hyperspherical harmonics [34] to fit 2n transfer data and found that of the two configurations in that model the "dineutron" configuration was dominant over the "cigar-like" configuration. Proton-^{6}He elastic scattering data of Alkhazov et al. [35] at 717 MeV/nucleon were fitted by them

10

with separate density distributions for the α-particle core and the valence neutrons. For two sets of their distributions they determined separate radii for the valence neutrons alone (2.97 ± 0.24 fm) and for all the neutrons (2.48 ± 0.11 fm), which gives a difference of 0.49 ± 0.26, in agreement with the result of our elementary analysis above. They also found 2.30 ± 0.07 fm for the rms radius of all the nuclear matter. Al-Khalili and Tostevin [36] showed that inclusion of correlations among the projectile and target constituents increased the size of the rms matter radius, from 2.30 fm [35] to 2.50 fm in the case of ^{6}He [37]. In another fit to the data of Alkhazov et al. [35], Abu-Ibrahim, Fujimura and Suzuki [38] used a complete expansion of the Glauber amplitude instead of the oft-used optical limit approximation and got a matter radius of 2.51 fm. They also determined a radius for all of the neutrons--2.78 fm. However, Tomaselli et al. [39], applying the dynamic correlation model to the same data, got a smaller matter radius, 2.38 fm. Finally, Karataglidis et al. [40] could find no clear evidence for a neutron halo in ^{6}He in their analyses of p-^{6}He elastic scattering data at 70 MeV/nucleon [41] or in ^{6}Li(γ,π$^+$)^{6}He data [42, 43]. The first analysis used a fully-microscopic folding model and the second a DWIA model.

V. CORRELATION of the HALO NEUTRONS

If the two halo neutrons in ^{6}He are correlated in their motion, sudden dissociation of ^{6}He will preserve the vector momenta of the neutrons and allow the correlation to be observed in the laboratory. An extreme example occurs when the two neutrons have the same space coordinates, hence, a "dineutron." Sudden dissociation will, in this case, reveal an α-particle moving in one direction and two neutrons with identical momenta in the opposite direction. The angle $θ_{nn}$ between the neutrons will, of course, be zero. We have two methods, using independent sets of data, with which to look for a correlation.

One method applies conservation of momentum to the momentum distributions of the preceding section. Conservation of momentum requires the momentum of the α-particle in ^{6}He to be balanced by the momentum of the two neutrons. It follows then that the widths of the α-particle and neutron distributions should be related. Applying the law of cosines to the triangle formed by the three momentum vectors gives

$$2p(n_1) \cdot p(n_2) = p_α^2 - [p_{n1}^2 + p_{n2}^2]. \qquad (7)$$

Averaging, and noting that Gaussians have $\langle p_x^2 \rangle = \langle p_y^2 \rangle = \langle p_z^2 \rangle = σ^2$, so that $\langle p^2 \rangle = 3σ^2$, gives:

$$(2/3)\langle p(n_1) \cdot p(n_2) \rangle = σ_α^2 - 2σ_n^2 \text{ and} \qquad (8)$$

11

$$\sigma_\alpha / \sigma_n = \sqrt{2 + (2/3)\langle p(n_1) \bullet p(n_2)\rangle / \sigma_n^2} \qquad (9)$$

We apply Eq. 9 to three special cases:

Case 1. The two neutrons form a dineutron. Then $p(n_1) = p(n_2)$, $\langle p(n_1) \bullet p(n_2)\rangle$ becomes $\langle p_n^2 \rangle = 3\sigma_n^2$, and $\sigma_\alpha / \sigma_n = 2$.

Case 2. The two neutrons are not correlated, i.e., $\langle p(n_1) \bullet p(n_2)\rangle = 0$. $\sigma_\alpha / \sigma_n = \sqrt{2}$.

Case 3. The two neutrons and the α-particle are emitted in accord with the 3-body phase-space model. This model is not a model of zero correlation; momentum conservation forces a correlation. It was shown by Sackett et al. [44] that $\langle p(n_1) \bullet p(n_2)\rangle$ is negative, with the consequence that $\sigma_\alpha / \sigma_n < \sqrt{2}$. In fact [44],

$$\langle p(n_1) \bullet p(n_2)\rangle = -E_d[m_n^2/(2m_n + m_\alpha)]; \qquad (10)$$

E_d is the decay energy, the sum of the kinetic energies of the three particles, and m_n and m_α are the neutron and α-particle masses. A typical value of E_d is 1.8 MeV [45]. With σ_n in Table II ranging from 26.9 MeV/c for the C target to 19.5 MeV/c for the U target, Eq. 9 gives $\sigma_\alpha / \sigma_n = 1.32$ to 1.23.

The values of σ_α / σ_n for the six targets and for Cases 1 and 2 are shown in the bottom part of Fig. 5. Case 1, where $\theta_{nn} = 0$ and $\sigma_\alpha / \sigma_n = 2$, is not supported by Fig. 5. The data fluctuate near, but not around, the uncorrelated value, $\sqrt{2}$, so the halo neutrons are not completely uncorrelated, but the correlation of Case 3 is below the data.

In the other method we look directly at the θ_{nn}, or the $\cos(\theta_{nn})$, distribution function. The events in this set are sparse since each event has an α-n-n triple coincidence. The measured cos θ_{nn} distribution functions for the six targets [45] are statistically equivalent. To reduce the fluctuations we summed the distributions, and that sum is shown in Fig. 6. The response of the detection system distorts the true cos θ_{nn} distribution. For example, the solid-angle acceptance of the system favors breakups with small values of θ_{nn}. To take that response, finite resolution, cross talk and other effects into account in comparing two theoretical models with experiment, we folded all effects with each theoretical cos θ_{nn} distribution in a Monte-Carlo simulation. The dashed histogram in Fig. 6, for the dineutron model, is strongly forward peaked; without the detector response it would be a delta function at cos $\theta_{nn} = 1$. The solid histogram is for the 3-body phase-space model. In that model momentum conservation and α-particle recoil force a correlation in which the average value of cos θ_{nn} is somewhat less than 90°[44]. With Eq. 10 and the approximation $\langle p(n_1) \bullet p(n_2)\rangle = \langle p_n^2 \rangle \langle \cos\theta \rangle$, $\langle \cos\theta \rangle \cong -0.2$. The model calculation shows

this effect, but the data do not. As in Fig. 5 for σ_α/σ_n, the dineutron model is also not favored by the $\cos\theta_{nn}$ data of Fig. 6, but there is a tendency towards it. This may be evidence for the hybrid model [46], a model in which the two valence neutrons of ^{6}He stay in shell-model orbits when they are close to the core, but form a cluster (dineutron) when they are far from the core. If the

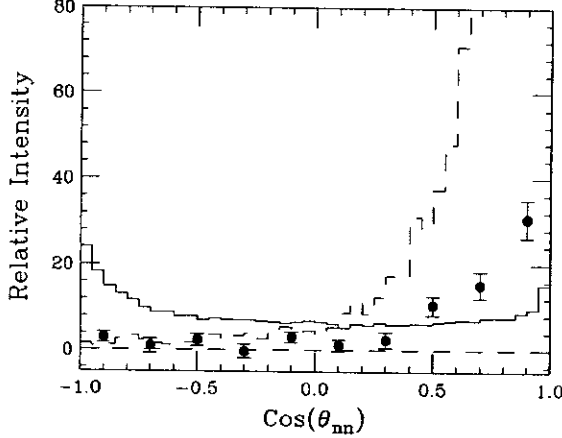Fig. 6. Distribution of angle between the two neutrons from ^{6}He breakup. The points are from 2n-α coincidence events for the six targets used in the experiment. The angle was calculated in the (2n + α) CM frame. The solid histogram is a Monte-Carlo simulation with the 3-body phase space model, and the dashed line is the same simulation with the dineutron model. The dashed line reaches above 10,000 at $\cos\theta = 1$.

^{6}He nucleus breaks up when the neutrons are far from the core, the neutrons tend to be strongly correlated. If the ^{6}He breaks up when the neutrons are close to the core, the neutrons tend to be uncorrelated.

VI. DIPOLE STRENGTH FUNCTION

In Sec. III. we saw that with targets of Pb and U most of the 2-n removal cross section of ^{6}He is Coulomb induced. For each such event the final-state kinematics gave us the decay energy E_d and, therefore, the energy of the photon absorbed, resulting in some information on the dipole strength function $dB(E1)/dE_x$ through the following relation [29] to the measurable spectral function $d\sigma_{E1}/dE_d$:

$$\frac{dB(E1)}{dE_d} = \frac{9\hbar c}{16\pi^3} \frac{1}{n_{E1}(E_\gamma)} \frac{d\sigma_{E1}}{dE_d} \tag{11}$$

In this equation $E_\gamma = E_x = S_{2n} + E_d$, and $n_{E1}(E_\gamma)$ is the number of equivalent E1 photons with energy E_γ surrounding the target nucleus. For ^{6}He the value of S_{2n} is 0.975 MeV. From vector momentum measurements of each of the three decay products, the decay energy was calculated for each 2n-α coincident event, and a measured spectral function was constructed. The function $d\sigma_{E1}/dE_d$ in Eq. 10 differs from the measured function in two respects. The measured function contains distortions introduced by the detection system, and it contains both Coulomb and nuclear

contributions. In computer simulations using the detector response function, the distortions were removed. Table I and Fig. 3 show that, for the U target, 2/3 of σ_{-2n}, or 1.25 b, is Coulomb induced. We used this value to normalize the dipole strength function determined with the U target, and we assumed that the shape of the function was not significantly altered by the nuclear part. The result is shown in Fig. 7, where the shaded area gives the range allowed by the statistical uncertainty in $d\sigma_{E1}/dE_d$. The function agrees with that determined by Aumann et al. [16] for ^{6}He projectiles at 240 MeV/nucleon. The dashed curve in Fig. 7 comes from a 3-body model [47] based on a hyperspherical harmonics approach. The dot-dashed curve, which is normalized to our peak, also comes from a 3-body model, and the authors [48] present a simple algebraic formula that gives an excellent approximation to the exact expression for the shape of the strength function. The
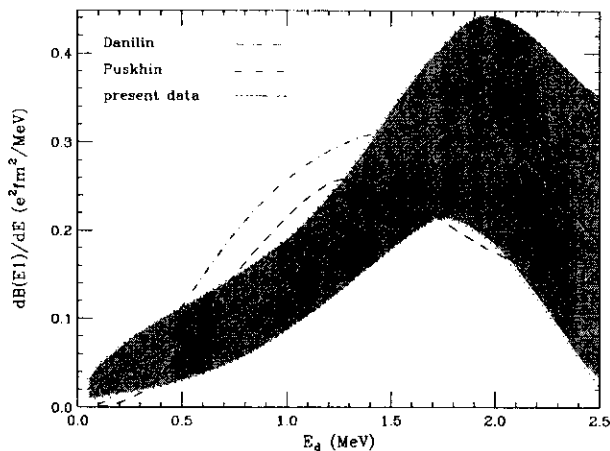

Fig. 7. Dipole strength function. Shaded area determined from the U data. Dashed curve [47] and dot-dashed curve [48] from two 3-body models.

experiment and the calculations agree that there is a strong concentration of the dipole strength at low energy, $E_d \sim 1.25 - 2.5$ MeV.

VII. SUMMARY

The dissociation reaction ^{6}He $\rightarrow \alpha + 2n$ was studied with ^{6}He projectiles at 23.9 MeV/u in targets of C, Al, Cu, Sn, Pb and U. Relative to Al, the 2n removal cross section σ_{-2n} with each of the other targets was determined. They were systematically higher in comparison to one model calculation [18] and systematically lower in comparison to another [25]. For a Pb target, values of total reaction cross sections σ_R [18] were available for comparison with our value of (1.70 ± 0.10) b through a prediction of the core-2n model [26] that $\sigma_{-2n}(^6\text{He}) = \sigma_R$ (^{6}He)- $\sigma_R(\alpha)$. The difference of the reaction cross sections [18], 1.82 ± 0.13, agrees with our

directly-measured value.

To determine the separate nuclear and Coulomb parts of the dissociation we applied our measured values of σ_{-2n} to $\sigma_{-2n} = \sigma_{nuclear} + \sigma_{coulomb} = a(1.2A^{1/3} + 2.6) + bZ^{1.8}$. For U, the Coulomb part accounts for 2/3 of σ_{-2n}.

Widths of the α-particle and neutron parallel momentum distributions decrease with target Z, perhaps indicating a weakening of the validity of the sudden approximation as Coulomb dissociation becomes important. The α-particle width for ^{6}He dissociation on C gave $\sigma_\alpha = (40.2 \pm 2.3)$ MeV/c, corresponding to a rms halo radius of (2.95 ± 0.17) fm, (0.35 ± 0.17) fm larger than the rms radius of all four neutrons [27,28].

Conservation of momentum requires a relationship between the α-particle and neutron momentum distributions and between the widths of those distributions. The observed relation indicates only a small correlation between the two neutrons, and this conclusion is supported by the distribution function for the angle between the two neutrons, which was obtained in n-n-α kinematically complete measurements.

The kinematically-complete measurements with the U target, for which the dissociation is 2/3 Coulomb, also yielded an E1 strength function up to ~ 2.5 MeV, and it agreed with one determined in an experiment at ten times our beam energy [16].

----

[1] I. Tanihata, H. Hamagaki, O. Hashimoto, S. Nagamiya, Y. Shida, N. Yoshikawa, O. Yamakawa, K. Sugimoto, T. Kobayashi, D.E. Greiner, N. Takashashi, and Y. Nojiri, Phys. Lett. **B160**, 380 (1985).

[2] T. Kobayashi, O. Yamakawa, K. Omata, K. Sugimoto, T. Shimoda, N. Takahashi, and I. Tanihata, Phys. Rev. Lett. **60**, 2599 (1988).

[3] A.B. Migdal, Yad. Fiz. **16**, 427 (1972); English translation Sov. J. Nucl. Phys. **16**, 238 (1973).

[4] P.G. Hansen and B. Jonson, Europhys. Lett. **4**, 409 (1987).

[5] I. Tanihata, Nucl. Phys. **A478**, 795c (1988).

[6] I. Tanihata, Nucl. Phys. **A522**, 275c (1991).

[7] T. Kobayashi, S. Shimoura, I. Tanihata, K. Katori, K. Matsuta, T. Minamisono, K. Sugimoto, W. Müller, D. L. Olson, T.J.M. Symons and H. Wieman, Phys. Lett. **B232**, 51 (1989).

[8] T. Kobayashi, in *Proc. First Interml. Conf. on Radioactive NuclearBeams, Berkley, 1989*, ed. W.D. Myers, J.M. Nitschke, and E.B. Norman (University of California, Berkley), p. 325.

[9] T. Kobayashi, Nucl. Phys. **A538**, 343c (1992).

[10] T. Kobayashi, Nucl. Phys. **A553**, 465c (1993).

[11] D. P. Balamuth, K. A. Griffioen, J. E. Bush, K. R. Pohl, D. O. Handzy, A. Aguirre, B. M. Sherrill, J. S. Winfield, D. J. Morrissey, and M. Thoennessen, Phys. Rev. Lett. **72**, 2355 (1994).

[12] P.G. Hansen, A.S. Jenson and B. Jonson, Annu. Rev. Nucl. Part. Sci. **45**, 591 (1995).

[13] Isao Tanihata, J. Phys. G:Nucl. Part. Phys. **22**, 157 (1996).

[14] R. E. Warner, R. A. Patty, P. M. Voyles, A. Nadasen, F. D. Becchetti, J. A. Brown, H. Esbensen, A. Galonsky, J. J. Kolata, J. Kruse, M. Y. Lee, R. M. Ronningen, P. Schwandt, J. von Schwarzenberg, B. M. Sherrill, K. Subotic, J. Wang, and P. Zecher, Phys. Rev. C **54**, 1700–1709 (1996).

[15] L.V. Chulkov et al., Phys. Rev. Lett. **79**, 201 (1997).

[16] T. Aumann et al., Phys. Rev. C **59**, 1252 (1999).

[17] S. Nakayama, T. Yamagata, H. Akimune, I. Daito, H. Fujimura, Y. Fujita, M. Fujiwara, K. Fushima, T. Inomata, H. Kohri, N. Koori, K. Takahisa, A. Tamii, M. Tanaka and H. Toyokawa, Phys. Rev. Lett. **85**, 262 (2000).

[18] R.E. Warner, M.H. McKinnon, N.C. Shaner, F.D. Becchetti, A. Nadasen, D.A. Roberts, J.A. Brown, A. Galonsky, J.J. Kolata, R.M.Ronningen, M. Steiner, and K. Subotic, Phys. Rev. C **62**, 024608 (2000).

[19] B. M. Sherrill, D.J. Morrissey, J.A. Nolen and J.A Winger, Nucl. Instru. Methods Phys. Res. B, **56&57**, 1106 (1991).

[20] D. Swan, J. Yurkon, D.J. Morrissey, Nucl. Instr. & Meth. **A348**, (1994) 314.

[21] P.D. Zecher, A. Galonsky, J.H. Kruse, S.J. Gaff, J. Ottarson, J. Wang, F. Deák, Á. Horváth, Á. Kiss, Z. Seres, K. Ieki, Y. Iwata and H. Schelin, Nucl. Instr. and Meth. **A401**, 329 (1997).

[22] J.J. Kruse, A. Galonsky, C. Snow, J. Wang, K. Ieki, Y. Iwata and P.D. Zecher, Nucl. Instr. & Meth., A, March (2002).

[23] G.F. Bertsch, B.A. Brown, and H. Sagawa, PRC 39, 1154 (1989).

[24] C.W. de Jaeger, H. de Vries and C.de Vries, At. Data Nucl. Data Tables **14**, 479 (1974).

[25] L.S. Ferreira, E. Maglione, J.M. Bang, I.J. Thompson, B.V. Danilin, M.V. Zhukov and J.S. Vaagen, Phys. Lett. B **316**, 23 (1993).

[26] Y. Ogawa, K. Yabana, and Y. Suzuki, Nucl. Phys. **A543**, 722 (1992).

[27] I. Tanihata, T. Kobayashi, O. Yamakawa, S. Shimoura, K. Ekuni, K. Sugimoto, N. Takahashi, T. Shimoda and H. Sata, Phys. Lett. **B206**, 592 (1988).

[28] I. Tanihata, D. Hirata, T. Kobyashi, S. Shimoura, K. Sugimoto and H. Toki, Phys. Lett. **B289**, 261 (1992).

[29] Carlos A. Bertulani and Gerhard Baur, Physics Reports **163**, 299 (1988).

[30] R. Serber, Phys. Rev. **72**, 1008 (1947).

[31] A. Csoto, Phys. Rev. C **48**, 165 (1993).

[32] K. Arai, Y. Suzuki and R.G. Lovas, Phys. Rev. C 59, 1432 1999).

[33] Yu.Ts. Oganessian, V.I. Zagrebaev and J.S. Vaagen, Phys. Rev. Lett. 82, 4996 (1999).

[34] M.V. Zhukov, B.V. Danilin, D.V. Fedorov, J.M. Bang, I.J. Thompson and J.S. Vaagen, Phys. Rep. **231**, 151 (1993).

[35] G.D. Alkhazov et al., Phys. Rev. Lett. **78**, 2313 (1997).

[36] J.S. Al-Khalili and J.A. Tostevin, Phys. Rev. Lett. **76**, 3903 (1996).

[37] J.S. Al-Khalili and J.A. Tostevin, Phys. Rev. C **57**, 1846 (1998).

[38] B. Abu-Ibrahim, K. Fujimura and Y. Suzuki, Nuc. Phys. **A657**, 391 (1999).

[39] M. Tomaselli, M. Hjorth-Jensen, S. Fritzsche, P. Egelhof, S. R. Neumaier, M. Mutterer, T. Kühl, A. Dax and H. Wang, Phys. Rev. C **62**, 067305 (2000).

[40] S. Karataglidis, P. J. Dortmans, K. Amos and C. Bennhold, Phys. Rev. C **61**, 024319 (2000).

[41] A.A. Korsheninnikov et al., Nuc. Phys. **A617**, 45(1997).

[42] K. Shoda, O. Sasaki and T. Kohmura, Phys. Lett. **101B**, 124 (1981).

[43] J. Shaw, T. Kobayashi, W. Clayton, L. Ghedira, D. Myers, P. Stoler, P. K. Teng and E. J. Winhold, Phys. Rev. C **43**, 1800 (1991).

[44] D. Sackett, K. Ieki, A. Galonsky, C. A. Bertulani, H. Esbensen, J. J. Kruse, W. G. Lynch, D. J. Morrissey, N. A. Orr, B. M. Sherrill, H. Schulz, A. Sustich, J. A. Winger, F. Deák, Á. Horváth, Á. Kiss, Z. Seres, J. J. Kolata, R. E. Warner, and D. L. Humphrey, Phys. Rev. C **48**, 118 (1993), see pp. 132-133.

[45] Jing Wang, Ph.D. thesis, Michigan State University (1999).

[46] K. Ikeda, Nucl. Phys. **A538**, 355c (1992).

[47] B.V. Danilin, I.J. Thompson, J.S. Vaagen and M.V. Zhukov, Nucl. Phys. **A 632**, 383 (1998).

[48] A. Pushkin, B. Jonson and M.V. Zhukov, J. Phys. G: Nucl. Part. Phys. **22**, L95 (1996).